A Vibrational Sum Frequency Spectroscopy Study of the Liquid−Gas Interface of Acetic Acid−Water Mixtures: 1. Surface Speciation

C. Magnus Johnson

Division of Corrosion Science, Royal Institute of Technology, Drottning Kristinas Väg 51, SE-100 44 Stockholm, Sweden

Eric Tyrode*

Department of Chemistry, Surface Chemistry, Royal Institute of Technology, Drottning Kristinas Väg 51, SE-100 44 Stockholm, and YKI, Institute for Surface Chemistry, Stockholm, Sweden

Steve Baldelli

Department of Chemistry, University of Houston, Texas 77204

Mark W. Rutland

Department of Chemistry, Surface Chemistry, Royal Institute of Technology, Drottning Kristinas Väg 51, SE-100 44 Stockholm, and YKI, Institute for Surface Chemistry, Stockholm, Sweden

Christofer Leygraf

Division of Corrosion Science, Royal Institute of Technology, Drottning Kristinas Väg 51, SE-100 44 Stockholm, Sweden

Received: June 18, 2004; In Final Form: October 15, 2004

Aqueous acetic acid solutions have been studied by vibrational sum frequency spectroscopy (VSFS) in order to acquire molecular information about the liquid−gas interface. The concentration range 0−100% acetic acid has been studied in the CH/OH and the C−O/C═O regions, and in order to clarify peak assignments, experiments with deuterated acetic acid and water have also been performed. Throughout the whole concentration range, the acetic acid is proven to be protonated. It is explicitly shown that the structure of a water surface becomes disrupted even at small additions of acetic acid. Furthermore, the spectral evolution upon increasing the concentration of acetic acid is explained in terms of the different complexes of acetic acid molecules, such as the hydrated monomer, linear dimer, and cyclic dimer. In the C═O region, the hydrated monomer is concluded to give rise to the sum frequency (SF) signal, and in the CH region, the cyclic dimer contributes to the signal as well. The combination of results from the CH/OH and the C−O/C═O regions allows a thorough characterization of the behavior of the acetic acid molecules at the interface to be obtained.

1. Introduction

Understanding surface tension and adsorption behavior in terms of molecular composition and conformation are some of the surface scientists' prime interests. To this end, carboxylate molecules have been extensively studied at a range of interfaces, and often, it is the hydrocarbon chain length which is varied to study, for example, the adsorption behavior. It has been less traditional to study the headgroup itself. Because acetic acid is the shortest alkyl carboxylate, it provides a good starting point for a fundamental exploration of the formation of Gibbs monolayers at the water−gas interface. Acetic acid is fully miscible with water (unlike many of the longer-chain homologues), but its intrinsic anisotropy, having a carboxyl headgroup and an alkyl chain consisting of a single methyl group, makes it nonetheless slightly surface-active. Thus, in solution, acetic acid is expected to display both the characteristics of a binary mixture over the entire concentration range (unlike a surfactant, which will form micelles and liquid crystalline phases at higher concentrations) and concentration-dependent interfacial behavior.

Acetic acid is also commonly associated with the degradation of materials, for example, by atmospheric corrosion in indoor environments.[1,2] The reason is that organic molecules undergo oxidation in ambient atmospheric environments, which frequently results in acetic acid as an end product.[3] A typical concentration of acetic acid in an indoor environment is around 20 ppb,[4] and thus, acetic acid is among the most dominant indoor corrosion promoters on metals. Metals exposed to an indoor environment are covered by several layers of water because of adsorption from humid air. This layer acts as a medium for chemical reactions and also as a solvent for gases. When molecules of acetic acid take part in an atmospheric corrosion process, they first have to penetrate the water−air interface, before reaching the metal surface. Thus, a typical corrosion process in an indoor environment involves two

* Corresponding author. Fax: + 46 8 208998. E-mail: eric.tyrode@surfchem.kth.se.

10.1021/jp047338q CCC: $30.25
Published on Web 12/03/2004

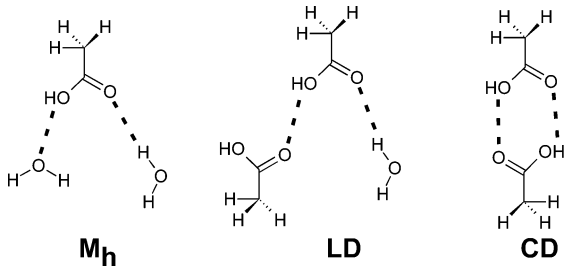

Figure 1. Three species of acetic acid. M_h = hydrated monomer; LD = linear dimer; CD = cyclic dimer. The nature of the hydrogen bonding of the carboxylic group is also illustrated schematically.

interfaces, the metal−water interface where the corrosion process takes place, and the water−air interface, studied in this report. Knowledge of the interfacial behavior of acetic acid in the interfacial region between a metal and its surrounding atmosphere is thus of great importance for a molecular understanding of acetic acid-induced atmospheric corrosion.

Acetic acid in the gas, liquid, and solid phases, as well as aqueous solution, has been studied extensively by IR[5−7] and Raman[8−12] spectroscopy in order to obtain information about the bulk phase. At low concentrations in water, acetic acid is partly dissociated to the carboxylate anion. For example, at a bulk concentration of 0.5 mole % (hereafter written only as %, because all concentrations are discussed in terms of mole %), approximately 99% of the acetic acid is protonated.[13] Above this concentration, there are three predominant species present:[8,14,15] hydrated monomers (M_h), linear dimers (LD), and cyclic dimers (CD), shown in Figure 1.

Similar findings were also made by Génin et al., who studied deuterated derivatives of acetic acid in heavy water by IR and Raman spectroscopy:[16] At concentrations up to roughly 2% acetic acid, the hydrated monomer is the only species in the solution. At concentrations less than 30%, linear dimers were detected, and their concentration increased to a maximum at 50%, where the solution contained hydrated monomers and similar amounts of linear and cyclic dimers. Above this concentration, the fraction of cyclic dimers increased, while the concentrations of linear dimers and hydrated monomers decreased. A small quantity of longer hydrogen-bonded chains was also present. In pure acetic acid, the cyclic dimer was found to be the dominant species. All three species have been identified by Raman spectroscopy, and the enthalpy changes in the conversions of $2M_h \leftrightarrow$ LD and LD $\leftrightarrow$ CD have been determined.[17] It is presumed that these bulk phase species are able to partition to the liquid−gas interface, but clearly, the surface concentrations will not necessarily reflect the bulk values. Semmler et al. also explained the characteristics of acetic acid solutions in terms of monomers and dimers.[8] They report that the cyclic dimers dominating at high concentrations break up upon addition of water, to form non-, mono-, and dihydrated linear dimers. In contrast, Nishi et al. favor a description of acetic acid solutions as consisting of two microphases, one water cluster phase and one acetic acid cluster phase,[18] and they also consider that chain clusters form instead of cyclic dimers in pure liquid acetic acid.[10] However, the common view is that acetic acid consists of monomers and linear and cyclic dimers as discussed already.

A comprehensive list of vibrational frequencies for acetic acid and its deuterated derivatives dates from the work of Haurie et al.,[19] obtained from both Raman and IR spectroscopy. The frequencies are summarized in Table 1. Unless otherwise stated, the mixture is in the liquid phase. All vibrations are stretching vibrations.

TABLE 1: Vibration Frequencies of Various Normal Modes of Acetic Acid[a]

vibration	IR (cm^{-1})	Raman (cm^{-1})
C−O	1295[19]	1283[19]
C═O (M, M_h)	1711[16 b] (M_h)	1790[8] (M, glacial)
	1788[5] (M, g)	1711[16 b] (M_h,)
		1788[5] (M, g)
C═O (LD1)	1745[16 b]	1762[8], 1746[16 b]
C═O (LD2)	1695[16 b]	1717[8], 1695[16 b]
C═O (CD)	1694[16 b]	1670[8], 1645[16 b]
$\nu_s(CH_3)$	2944 (g)[20]	2949[19]
$\nu_a(CH_3)$	2996 (g)[20]	3000[19]
$\nu_s'(CH_3)$	3051 (g)[20]	3032[19]

[a] M = monomer, M_h = hydrated monomer, CD = cyclic dimer, LD1 = free carbonyl group of linear dimer, LD2 = hydrogen-bonded carbonyl group of linear dimer, g = gas phase. [b] CH_3COOD in D_2O.

Sims et al. have performed an extensive study of aqueous acetic acid solutions by measuring a variety of static and dynamic properties.[21] At a concentration of 5% acetic acid, the enthalpy of mixing exhibits a minimum, indicating that the solution has maximum order. At around 11% acetic acid, carbon-13 NMR chemical shift, carbon-13 spin−lattice relaxation time, microwave absorption, and specific conductance show evidence of a major structural change, and it is inferred that the dihydrated acetic acid monomer dominates at concentrations lower than 11% acetic acid. At approximately 55% acetic acid, a structural change is detected as a maximum in density, molar enthalpy of mixing, index of refraction, and relative viscosity. This is interpreted as the formation of cyclic dimers from linear dimers as the acetic acid concentration increases above 55%.

Because our studies include experiments with aqueous acetic acid solutions, it is also important to review the spectroscopic properties of water. Many studies of pure water have been performed by vibrational spectroscopy, including IR,[22,23] Raman,[24,25] and sum frequency,[26,27] just to mention a few. The sum frequency (SF) spectrum of water shows prominent features at ∼3250, ∼3450, and ∼3700 cm^{-1}. These peaks have been respectively attributed to symmetrically and asymmetrically hydrogen-bonded water and free OH stretching vibrations. The free OH stretch originates from non-hydrogen-bonded OH groups protruding out into the gas phase. The broad band with prominent features at ∼3250 and ∼3450 cm^{-1} is also present in Raman spectra.

Despite the extensive studies of the bulk behavior of acetic acid solutions, information about the liquid−gas interface has not been obtained so far. In this study, the C−O, C═O, C−H, and O−H stretching vibrations of acetic acid and the OH stretches of water have been studied by vibrational sum frequency spectroscopy (VSFS) in the concentration range 0−100%. The spectra provide information about the concentration-dependent surface behavior of acetic acid and water. To explain the spectral features in more detail, the knowledge of the different species of acetic acid discussed already has been used. The following paper in this issue further explores the interface of aqueous acetic acid solutions and provides an orientation analysis of interfacial acetic acid and water molecules.

2. Theory

VSFS (or sum frequency generation, SFG) is a second-order nonlinear laser spectroscopic technique well-suited for interfacial studies. The theory has been extensively treated in other sources,[27−31] and only a summary of the most important

concepts is presented here. VSFS can be applied to all interfaces accessible by light, for example, the liquid−gas, solid−liquid, and liquid−liquid interfaces. The technique utilizes two pulsed laser beams, one at a fixed visible frequency and one that is tuneable in the IR region. These beams overlap in time and space at the interface, and a third beam with the sum frequency of the two incident beams is emitted, $\omega_{SFG} = \omega_{vis} + \omega_{IR}$. During the SF process, the energy and momentum of the radiation are conserved. The SF process can be viewed as a resonant IR absorption followed by a nonresonant Raman process, meaning that a molecule must be both IR and Raman active in order to give rise to sum frequency generation. VSFS can only detect molecules with a net orientation (i.e., not isotropically distributed), and the surface specificity of VSFS arises from the fact that a second-order process can only occur in noncentrosymmetric media under the electric dipole approximation. In contrast to isotropic bulk media, interfaces are noncentrosymmetric, from which it follows that it is possible to distinguish molecules at the interface from the vast excess of the same molecules in the bulk.

The intensity of the sum frequency signal is proportional to the square of the surface nonlinear polarization, which in turn is related to the surface nonlinear susceptibility, according to eq 1[32]

$$I_{SFG} \propto |P_{SFG}|^2 \propto |\chi^{(2)}|^2 I_{vis} I_{IR} L_{SFG}^2 K_{IR}^2 K_{vis}^2 \qquad (1)$$

where I_{SFG} is the sum frequency intensity, P_{SFG} is the induced surface nonlinear polarization, $\chi^{(2)}$ is the macroscopic second-order nonlinear susceptibility, I_{vis} and I_{IR} are the intensities of the visible and IR beams, respectively, and L_{SFG}, K_{IR}, and K_{vis} are the Fresnel factors. The nonlinear susceptibility has a nonresonant contribution primarily related to the polarizability of the interfacial molecules and resonant contributions from vibrational modes of the interfacial molecules, according to eq 2

$$\chi^{(2)} = \chi_{NR}^{(2)} + \sum_n \chi_{R,n}^{(2)} \qquad (2)$$

where $\chi_{NR}^{(2)}$ is the nonresonant part, and $\chi_{R,n}^{(2)}$ are the resonant parts of the susceptibility. For a dielectric surface, as in our case, $\chi_{NR}^{(2)}$ is real.[33] Because of the coherent nature of the sum frequency process, it is possible to determine the average orientation of interfacial molecules by performing experiments with different polarization combinations. In this report, all experiments have been performed with the polarization combination ssp (s-polarized SF, s-polarized visible, and p-polarized IR beam, respectively), which in principle probes vibrations having a component perpendicular to the surface. Beams with s polarization are polarized perpendicular to the plane of incidence, and beams with p polarization are polarized parallel to the plane of incidence.

The nonlinear susceptibility is related to the orientationally averaged hyperpolarizability, described by eq 3

$$\chi_R^{(2)} = \frac{N}{\epsilon_0} \langle \beta_R^{(2)} \rangle \qquad (3)$$

where $\chi_R^{(2)}$ is the second-order nonlinear susceptibility corresponding to a vibrational resonance, N is the number of molecules, ϵ_0 is the dielectric permittivity, and $\langle \beta_R^{(2)} \rangle$ denotes the orientationally averaged molecular hyperpolarizability for a vibrational resonance. $\beta^{(2)}$ is related to the product of the Raman polarizability tensor component $\alpha_{\alpha\beta}$ and the IR transition dipole moment μ_γ, according to eq 4

$$\beta_{\alpha\beta\gamma}^{(2)} = \frac{\langle g|\alpha_{\alpha\beta}|v\rangle\langle v|\mu_\gamma|g\rangle}{\omega_n - \omega_{IR} - i\Gamma_n} \qquad (4)$$

where g is the ground state, v is an excited state, ω_{IR} is the frequency of the IR laser beam, ω_n is a vibrational transition frequency, i is the imaginary unit, and Γ_n is the damping constant. Equation 4 shows that the hyperpolarizability and thereby the SF intensity increase when the IR beam is in resonance with a vibrational transition. Note that caution must be taken when a beam is close to strong resonances (such as electronic transitions) of the molecules, because the perturbation might not be considered "small" under those conditions. The Bloch equations are therefore commonly used in nonlinear optics to describe strong interactions.[34]

3. Experimental Section

3.1. Sum Frequency Generation Spectrometer. In general terms, a pulsed Nd:YAG laser was used to pump an optical parametric generator /optical parametric amplifier (OPG/OPA) to produce both a visible beam at a fixed wavelength and a tuneable IR beam, which subsequently were directed toward the sample. The intensity of the SF beam generated at the surface was measured by a photomultiplier tube (PMT) and gated electronics. Finally, the normalized SF intensity was plotted against the IR wavenumber, generating the surface vibrational spectrum. A detailed description of each of the different elements follows.

3.1.1. Laser − OPG/OPA. The laser system employed consists of an active/passive mode-locked Q-switched Nd:YAG laser (Ekspla, PL2143A/20) with a fundamental output at 1064 nm, generating pulses with a length of ∼24 ps, a repetition rate of 20 Hz, and an approximate energy per pulse of 40 mJ. In the OPG/OPA (LaserVision), the fundamental is split into two separate beams. The first beam is frequency doubled in a nonlinear KTP crystal, thus producing radiation at 532 nm, part of which is used as the visible beam in the experiments, while the remaining part is used to pump the first stage of the OPG/OPA which consists of two angle-tuned nonlinear KTP crystals (type II phasematching). The resulting idler wave (710−860 nm) from this first stage is combined with the second part of the fundamental beam of 1064 nm for difference frequency mixing in a set of two angle-tuned nonlinear KTA crystals (type II phasematching). The output of this second stage is used in the experiments and is a mid-IR beam (1.4−5 μm) with a bandwidth of 7−9 cm^{-1} and a maximum energy per pulse between 800 and 70 μJ depending on the wavelength. For wavelengths longer than 5 μm (below 2000 cm^{-1}), a third OPA stage consisting of an angle-tuned $AgGaSe_2$ crystal is used (type I phasematching). The output of this final stage (5−12 μm), created by difference frequency mixing of the signal and idler waves from the second stage, has a slightly broader bandwidth (<15 cm^{-1}) and a maximum energy per pulse of 70 to 10 μJ, also wavelength-dependent. All angle-tuned nonlinear crystals are moved independently with 5 stepping motors controlled by a stand-alone computer, which is interfaced with the main acquisition program.

The generated visible and mid-IR beams are overlapped in time and space on the sample in a copropagating geometry, where the incident angles are 55° and 63° from the surface normal for the visible and IR beams, respectively. Before reaching the sample, the visible beam first passes through a

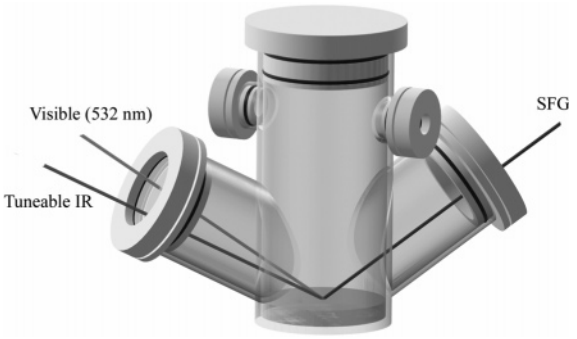

Figure 2. Sample cell used for the VSFS experiments. The visible and IR beams reflected from the liquid surface are not shown for clarity.

half-wave plate and a telescope to reduce the beam diameter to approximately 1.4 mm, with an approximate energy of 0.9 mJ/pulse. The IR beam is also first passed through a frequency-tuneable half-wave plate (Alphalas GmbH) and is focused down to a beam diameter of around 0.9 mm at the sample, while ensuring that the focal point is not at the surface of the sample but approximately 1 cm below (to avoid heating the surface). Tighter focus (0.5 mm diameter at the sample) of the IR beam was used for experiments below 2000 cm^{-1} to compensate for the reduced energy per pulse. The IR beam is confined to a box containing an overpressure of dry air for at least 95% of its path length, considerably reducing the IR losses in the absorption bands of water vapor.

3.1.2. Detection and Acquisition. The generated SF beam is first passed through a series of irises to spatially filter scattered light and then a band-pass filter (Omega Optical) and Notch Plus filter (Kaiser Optical Systems) before being focused toward a monochromator (Jobin Yvon) with a PMT (Hamamatsu R3788) attached at its exit. Gated electronics from Stanford Research Systems (SR250, SR245) allow discrimination of the PMT signal from the electronic background. The integrated signal is finally acquired in a computer and processed by a Labview (National Instruments) program. The tuning of the IR wavelength is carried out in a continuous mode, in which the IR frequency is scanned at a speed of 1 cm^{-1}/s. The IR and visible energy fluctuations are measured (Molectron energy meter EPM2000 with J5-09B probes) and later used for SF intensity normalization. The averaging is at the same rate as the detection of the SF beam. A scattering background is automatically recorded at the beginning of each scan by motorized blocking of the path of the IR beam. Stepping motors were also used to adjust the IR-tuneable half-wave plate and monochromator wavelength during the scan. At least 10 scans were carried out per concentration, giving an average of no less than 600 shots per point in the spectra shown. The experiments were performed at least three different times. Spectra were also normalized to account for polarization and wavelength dependence of the band-pass filter, Notch Plus filter, monochromotor, and PMT. The frequency of the tuneable IR beam was calibrated with a polystyrene film to ± 2 cm^{-1} using the standard CH and CC stretching absorption bands.

3.1.3. Cell and Sample Preparation. The sample was placed in a custom-designed cell, the major features of which can be seen in Figure 2.

The main body is made of glass, while the hollow lateral stoppers are machined in Teflon to accommodate CaF_2/BaF_2 and BK7 windows. Hermetic sealing is granted by Kalrez o-rings. The angles of the lateral arms match the incoming and outgoing angles of the IR and SF beams, respectively. The two smaller upper arms are used for IR normalization, where a small portion of the main IR beam is passed through to account for IR power fluctuations and gas-phase absorption. The beam path of the overhead is equal in distance to the one travelled by the main IR beam in the cell before reaching the sample. The cell is placed in a cooling bath, where temperature is controlled to within ± 0.2 °C and continuously monitored with a thermocouple located inside a capillary tube in direct contact with the sample (not shown in Figure 2). Proper mixing is ensured by a glass-coated magnetic stirrer. The cell was meticulously cleaned before experiment with a 50/50 mixture of concentrated sulfuric and nitric acid, followed by a thorough rinsing procedure with Milli-Q water. During this routine, filtered nitrogen was used to pump the different fluids in and out, with the cell closed, and thus never exposing the chamber to the air. The rest of the glassware used in the experiments was cleaned with bichromo-sulfuric acid for 24 h and then thoroughly rinsed with water.

All experiments were carried out at 4.0 ± 0.2 °C, which corresponds to supercooled conditions for pure acetic acid (mp 16.7 °C). This low temperature was preferred in order to reduce the gas-phase absorption of the IR beam before reaching the sample and avoid deterioration of the windows. Nevertheless, exploratory tests at room temperatures yielded the same results as observed at 4 °C.

TABLE 2: Experimentally Obtained SF Frequencies of Vibrations of Water, Acetic Acid, and Deuterated Water.

peak no.	ω_n (cm^{-1})	assignment
1	~1300	C—O stretch
2	~1720	C═O stretch
3	2740	free OD stretch (D_2O)
4	2950[a]	CH_3 symmetric stretch
5	~2975	H-bonded CH_3COOH
6	~3250	symmetrically H-bonded H_2O
7	~3420	asymmetrically H-bonded H_2O
8	~3620	weakly/non H-bonded H_2O
9	3702	free OH stretch (H_2O)

[a] This frequency corresponds to pure acetic acid. By decreasing acid concentration, the frequency decreases to 2943 cm^{-1} at 0.3%.

3.2. Substances. Glacial acetic acid (Aldrich, 99.99+%), acetic acid −d4 (CDN, 99.5%), and D_2O (CDN, 99.9%) were used as received. The 18.2 MΩ/cm water used in the experiments was obtained from a Millipore RiOs-8 and Milli-Q PLUS 185 purification system, filtered with a 0.2 μm Millipak filter. The total organic carbon content of the water was monitored with a Millipore A-10 unit and never exceeded 6 ppb in any of the measurements.

4. Results and Discussion

A total of nine different peaks have been analyzed in the various spectra. The frequencies obtained in the SF experiments and assignments of the water and acetic acid peaks are summarized in Table 2. All peaks originate from stretching vibrations.

4.1. The CH/OH stretching region (2680−3900 cm^{-1}). The ssp spectrum (only ssp spectra are reported in this paper) of water shown in Figure 3a is similar to that reported in other VSFS experiments.[26,27] Three prominent features are seen: the OH stretch of strongly hydrogen-bonded (symmetrically bonded) water at ~3250 cm^{-1}, the OH stretch of weaker hydrogen-bonded (asymmetrically bonded) water at ~3420 cm^{-1}, and the free OH at 3702 cm^{-1}. The spectrum of pure acetic acid is shown in Figure 3b, in which only one peak is present, the symmetric methyl stretch, $\nu_s(CH_3)$, at 2950 cm^{-1}, in agreement with the results in Table 1. The asymmetric peak shape of the free OH and $\nu_s(CH_3)$ originate from destructive interference with

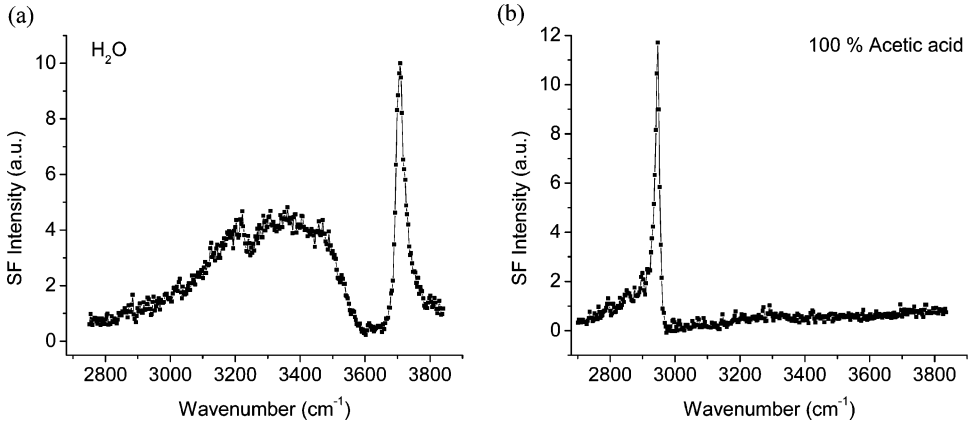

Figure 3. (a) SF spectrum of pure water. The peaks centered at ~3250 and ~3420 cm^{-1} correspond to hydrogen-bonded water, and the peak at 3702 cm^{-1} corresponds to the free OH. (b) SF spectrum of pure acetic acid. The peak at 2950 cm^{-1} is assigned to $\nu_s(CH_3)$. The lines are just guides to the eye.

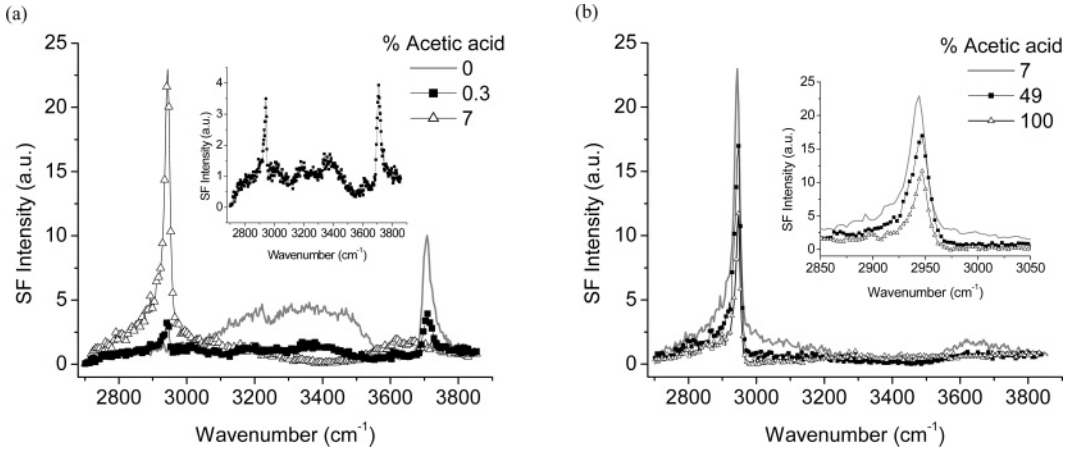

Figure 4. (a) SF spectra with ssp polarization in the low concentration range of aqueous acetic acid solutions. Pure water is shown as a reference. The inset is shown to make the features in the spectrum of 0.3% acetic acid clearer. (b) SF spectra with ssp polarization in the high concentration range of aqueous acetic acid solutions. The spectrum of 7% (same as in Figure 4a) is shown for reference. The inset is a magnification of the CH stretching region. The lines are just guides to the eye.

an adjacent peak at the low-wavenumber side for the free OH and destructive interference with the nonresonant background at the high-wavenumber side for $\nu_s(CH_3)$.

From IR studies, the OH stretch of pure hydrogen-bonded acetic acid is known to give rise to a broad band centered at ~3000 cm^{-1}.[6] The lack of this broad band in the SF spectrum of pure acetic acid is discussed in the following text.

Figure 4a shows three spectra of 0, 0.3, and 7% acetic acid. Uniquely for the spectrum of 0.3% acetic acid, all of the six peaks (peak numbers 4−9 in Table 2) encountered in the CH/OH region are seen (inset in Figure 4a), even though some are weak. At all other concentrations, at least one of the peaks is absent. It is further seen in the spectrum of 0.3% that the intensity in the spectral regions of hydrogen-bonded water and the free OH has decreased significantly compared to the spectrum of pure water, despite the small amount of acetic acid added. These features disappear at a concentration of 1.6% acetic acid (spectra not shown). It can also be observed that $\nu_s(CH_3)$ starts to appear at 0.3% and is present throughout the whole concentration region. The presence of the strong methyl peak indicates the preferential orientation of acetic acid at the interface. While it is not a priori possible to say whether the methyl groups point up or down, it is likely that the methyl groups point toward the gas phase. This is justified by the following argument: In order to minimize the free energy of the system, the polar end of the acetic acid molecule will tend to be directed into the polar bulk liquid phase,[35] and hence, the methyl group would tend to point into the gas phase. Evidence that the polar group points into the liquid phase is found from the fact that the free OH of acetic acid at 3583 cm^{-1} [20] is not seen at any concentration. Two other bands also appear at 0.3%: at 2975 cm^{-1}, a band superimposed on $\nu_s(CH_3)$ is seen, and also, a weak band at 3620 cm^{-1} is observed.

As for 1.6%, the peaks assigned to the OH stretch of hydrogen-bonded water and the free OH of water have totally vanished for 7% acetic acid and all higher concentrations, indicating that the acetic acid molecules have disrupted the hydrogen-bonding network of water in the interfacial region. This lack of signal can be used to infer the absence of ionized acetic acid surface species, as it has been observed previously that charged surface-active molecules will tend to orient more water molecules in the surface region because of the high electric field.[36,37] This ordering causes the SF signal of hydrogen-bonded water to increase in the 3000−3500 cm^{-1} range. Because this increase is not observed in these experiments, it indicates that the acetic acid is not ionized, which is consistent with its bulk behavior.[13] Moreover, the symmetric and antisymmetric carboxylate peaks originating from the acetate anion are not seen at any concentration, as will be discussed in a later section.

The intensity of $\nu_s(CH_3)$ in the spectrum of 7% acetic acid has increased significantly compared to the spectrum of 0.3%. When comparing the spectra in Figure 4a and b, it can be seen

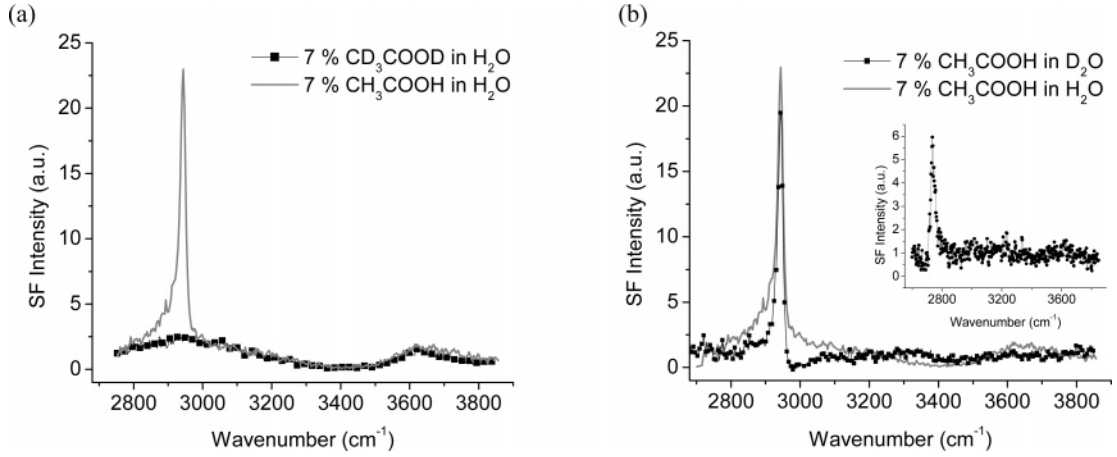

Figure 5. (a) SF spectra with ssp polarization of 7% CH_3COOH in H_2O and 7% CD_3COOD in H_2O. In the spectrum of CD_3COOD, $\nu_s(CH_3)$ is absent. (b) SF spectra with ssp polarization of 7% CH_3COOH in H_2O and 7% CH_3COOH in D_2O. The broad bands at ~2975 and 3620 cm^{-1} are absent in the spectrum of CH_3COOH in D_2O. The inset in (b) shows an SF spectrum of the free OD stretch of pure D_2O for reference. The lines are just guides to the eye.

that the intensity of $\nu_s(CH_3)$ decreases with increasing concentration above 7% acid. However, a quantitative study found in the following paper of this issue shows that the fitted amplitude of $\nu_s(CH_3)$ remains essentially constant throughout the concentration range, apart from 0.3% where it is lower. This is due to the fact that the broad band centered at ~2975 cm^{-1}, which decreases by increasing concentration above 7%, is superimposed on $\nu_s(CH_3)$. The bandwidth of $\nu_s(CH_3)$ is also constant, while the peak position changes slightly by concentration, from 2943 cm^{-1} at 0.3% to 2950 cm^{-1} at 100% acetic acid. Besides the symmetric methyl stretch, the broad bands at ~2975 and ~3620 cm^{-1} are clearly seen in the spectrum of 7% acetic acid.

The spectrum of 12% (not shown) is almost identical to that of 7% acetic acid, indicating that the surface structure remains almost constant over that concentration range. At concentrations higher than 12% acetic acid, many bands start to decrease in intensity, as seen in Figure 4b. At 49% acetic acid, the intensities of the broad bands centered at 2975 and 3620 cm^{-1} have decreased significantly, and at 100% acetic acid, they have disappeared. As mentioned already, the former of these bands has previously been studied by IR spectroscopy[6] and assigned to the OH stretch of hydrogen-bonded acetic acid. The latter band has been studied in liquid water by Raman spectroscopy, and resonances in the region 3620−3660 cm^{-1} have been ascribed to free OH oscillators.[38,39] In a VSFS study, a band at 3560 cm^{-1} has been assigned to weakly hydrogen-bonded OH oscillators of water.[40] A control experiment with deuterated derivatives of water and acetic acid has been performed to confirm the assignments of the bands at ~2975 and ~3620 cm^{-1}. Figure 5a displays two spectra, one of 7% CD_3COOD in H_2O and one of 7% CH_3COOH in H_2O for reference.

The two spectra in Figure 5a show striking similarities in the whole spectral range except that $\nu_s(CH_3)$ is absent in the spectrum of CD_3COOD as expected. Because the broad bands at 2975 and 3620 cm^{-1} are still present in the CD_3COOD spectrum, the conclusion can be drawn that the methyl group is not responsible for those spectral features. Figure 5b shows a spectrum of 7% CH_3COOH in D_2O and a spectrum of 7% CH_3COOH in H_2O for reference. There will be an exchange between the acidic hydrogen of the acid and the deuterons of D_2O, but because there is a vast excess of deuterons, the spectral features of the protonated acid will vanish. The inset in Figure 5b shows the free OD stretch of pure D_2O, which is red-shifted around 1000 cm^{-1} compared to the free OH of H_2O. In the main figure, it is seen that $\nu_s(CH_3)$ is still present, but the two broad bands at 2975 and 3620 cm^{-1} have vanished. Thus, we suggest that they originate from hydrogen bonding between CH_3COOH and H_2O as will be discussed. Therefore, the band at 2975 cm^{-1} is assigned to the OH stretch of hydrogen-bonded acetic acid, and the band at 3620 cm^{-1} is assigned to the OH stretch of weakly or non-hydrogen-bonded water. The decrease in intensity of the latter band at higher concentrations of acetic acid is explained by the fact that there are fewer water molecules available for hydrogen bonding.

4.2. The C−O/C═O Stretching Region (1080−1950 cm^{-1}). The C−O/C═O stretching region provides valuable information about the surface structure in combination with the information obtained from the CH/OH stretching region. The C═O stretching vibration was most extensively studied in this region because it gives rise to a much stronger signal than the C−O stretching vibration. Figure 6 shows spectra in the C−O/C═O region. The weak band centered at ~1300 cm^{-1} in Figure 6a for 7% acid is assigned to the C−O stretching vibration of acetic acid, in agreement with Raman and IR studies.[8,16,41] However, it is likely that the C−O stretch is coupled with other vibrations of the acetic acid molecule.[41] This band is only seen for a few concentrations and is always weak compared to the C═O band, which is explained by the lower IR and especially Raman cross-sections of the C−O stretch.

The bending mode of H_2O at ~1600 cm^{-1} [42] is not observed in pure water, nor in any mixture with acetic acid. This may be due to lower IR and Raman cross-sections compared to the stretching vibrations and also the fact that the transition dipole moment of the bending vibration is close to the surface plane. Other modes not detected are the deformation modes of the methyl group of acetic acid at ~1400 cm^{-1},[19,20] despite the fairly high IR and Raman cross-sections.

An important observation in Figure 6 is that there is only one C═O peak, located at 1720 cm^{-1} throughout the whole concentration region. The peak position of 1720 cm^{-1} is consistent with protonated acetic acid and confirms the idea discussed already that the surface species are undissociated. The acetate anion would be easily distinguished by the fact that it has two bands at 1423 and 1579 cm^{-1}, originating from the symmetric and antisymmetric carboxylate stretching vibrations, respectively[43] (the absorption region for the acetate anion is only shown in Figure 6a for 7% acetic acid, but no signs of acetate bands are seen at any concentration). The peak positions have

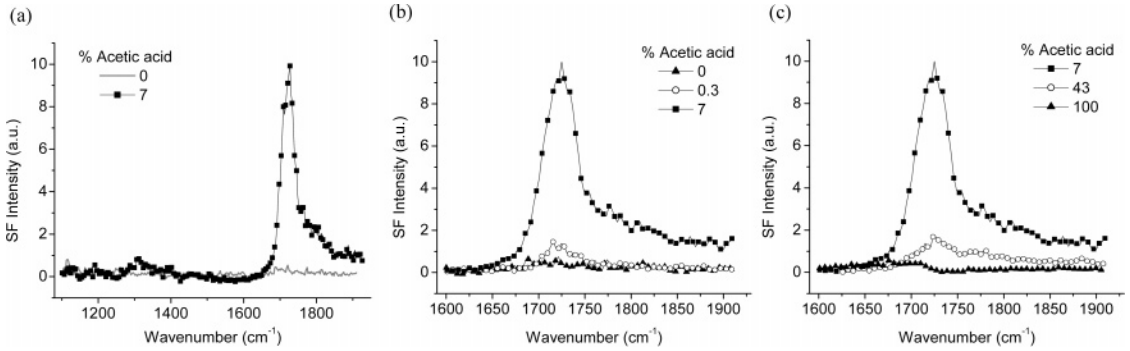

Figure 6. (a) SF spectra with ssp polarization of pure water and 7% acetic acid in water in the C−O/C═O region. (b) SF spectra with ssp polarization of pure water and 0.3% and 7% acetic acid. (c) SF spectra with ssp polarization of 7, 43, and 100% acetic acid. At the high wavenumber side of the C═O peak, constructive interference with the nonresonant background tends to increase the intensity of the tail. The lines are just guides to the eye.

been confirmed by a VSFS study of a fatty acid at the water−air interface, where the symmetric carboxylate stretch of the acetate anion was observed at 1420 cm^{-1} and the protonated species at 1720 cm^{-1}.[40]

Furthermore, the constant shape and bandwidth of ∼20 cm^{-1} of the C═O stretch in our experiments also shows that only one of the acetic acid species depicted in Figure 1 (M_h, LD, or CD) can be responsible for the SF signal throughout the whole concentration range where it was detected. The three species can be distinguished in IR and Raman spectroscopy by the position of the C═O peak as shown in Table 1. Hydrated monomers have the IR and Raman absorptions in close proximity to each other, and the same is true for the linear dimers. In contrast, the cyclic dimer has a splitting between the IR and Raman absorption frequencies, because the two corresponding modes belong to different symmetry species. This is due to the fact that the cyclic dimer is centrosymmetric, and the C═O stretch of the cyclic dimer would therefore not be expected in an SF spectrum. Therefore, the peak must originate from either the hydrated monomer or the linear dimer. Inspection of Figure 1 shows that two C═O peaks (hydrogen-bonded and free carbonyl group) would be expected for the linear dimer, favoring an assignment of the vibration to the hydrated monomer. This seems reasonable particularly in the view of the fact that at 0.3% acetic acid, only the hydrated monomer is present in the bulk.[16] A bulk concentration of 0.3% corresponds to 7% acetic acid at the surface,[44] and also at that concentration, the hydrated monomer would be dominant. There is no spectroscopic reason that linear dimers should not be observed in SF spectra, but the results presented here show no signs of linear dimers at the surface.

As seen in Figure 6b and c, the intensity of the C═O stretch increases up to 7% and then decreases at concentrations above 7% acetic acid. For concentrations higher than 43%, the C═O peak is not detected. Note, however, that in the spectrum of 100% acetic acid, there is a small feature in the C═O region. The disappearance of the C═O peak at higher concentrations is explained by the fact that at low concentrations, hydrated monomers, which dominate the bulk, reside at the surface and give rise to SF intensity. When the concentration of acetic acid increases, the cyclic dimer concentration will increase in the bulk and at the surface, leading to a decrease of the concentration of hydrated monomers. Because cyclic dimers are centrosymmetric, they will not give rise to any C═O signal. Thereby, the SF signal decreases until it totally vanishes at high concentrations of acetic acid, where the surface is dominated by cyclic dimers. The cyclic dimers are thus identified indirectly as the dominant surface species by the absence of the C═O peak in the spectrum, rather than by a characteristic peak.

The explanation why $\nu_s(CH_3)$ still shows some intensity at 100% acetic acid is that the methyl groups in the cyclic dimer are further apart than the C═O groups and thus reside in different environments: one methyl group points out into the gas phase and the other points into the bulk. Thus, even though the cyclic dimer is centrosymmetric in isolation, the centrosymmetry regarding the methyl groups is broken at the surface. Hence, the intensity of the $\nu_s(CH_3)$ peak is assumed to have contributions also from cyclic dimers. The increase in frequency of $\nu_s(CH_3)$ from 2943 to 2950 cm^{-1} throughout the concentration range 0.3−100% acid is also a proof of a change in the surface structure, despite the fact that it is not possible from the frequency change to judge what structural change has occurred.

The disappearance of the OH stretch of hydrogen-bonded acetic acid at ∼2975 cm^{-1} at high concentrations also supports the argument of cyclic dimer formation. The same signal cancellation as for the C═O stretch should also occur for this peak, because the SF signal of the hydrogen-bonded OH stretch of a cyclic dimer must vanish due to centrosymmetry. The OH stretch of hydrogen-bonded acetic acid is known from IR spectroscopy of pure acetic acid,[6] where it necessarily originates from acid−acid interactions. However, according to the earlier discussion, it follows that this band arises from water−acid interactions in hydrated monomers in our VSFS experiments.

Another argument to explain the decrease and absence of intensity of many bands at higher concentrations could be a change in orientation or an increase in disorder of the acetic acid molecules. However, an orientation analysis based on polarization experiments, reveals that such arguments can be neglected.[44] Reference 44 is a continuation of this paper and is concerned with calculations of the orientation of interfacial acetic acid molecules.

5. Conclusions

Several stretching bands of acetic acid and water have been observed by vibrational sum frequency spectroscopy (VSFS), and their concentration dependence have been studied. It has been concluded that even such small amounts as 0.3% acetic acid disrupt the water surface significantly. Furthermore, the spectral features of the two hydrogen-bonded peaks at ∼3250 and ∼3420 cm^{-1}, and the free OH at 3702 cm^{-1}, characteristic of a pure water surface, already disappear at a concentration of 1.6% acetic acid. The dominating spectral features at concentrations higher than 1.6% are the symmetric methyl stretch of acetic acid at 2943−2950 cm^{-1} (depending on concentration), the OH

stretch of hydrogen-bonded acetic acid at ~2975 cm^{-1}, the OH stretch of weakly or non-hydrogen-bonded water at ~3620 cm^{-1}, and the C═O stretch of acetic acid at 1720 cm^{-1}. At concentrations higher than 49%, the OH stretch of hydrogen-bonded acetic acid and the OH stretch of weakly or non-hydrogen-bonded water disappear, and at concentrations higher than 43%, the C═O stretch vanishes. The interfacial acetic acid molecules have been determined to be protonated in the whole concentration range studied. In the C═O region, the hydrated acetic acid monomer has been favored over the cyclic and linear dimers to give rise to the SF signal. However, because of its centrosymmetry, the cyclic dimer gives rise to indirect information through the absence of absorption bands in the C═O region. In the CH region, the hydrated monomer and the cyclic dimer are determined to contribute to the SF signal. The C—O stretching vibration at ~1300 cm^{-1} has been reported for a few concentrations as a weak band. A theoretical analysis of the orientation of the interfacial acetic acid molecules is presented in the following paper in this issue.

Acknowledgment. Financial support from the Swedish Research Council (VR), the Swedish Research Council for Engineering Sciences (TFR), and the Swedish Foundation for Strategic Research (SSF) are gratefully acknowledged. We thank Dr. Colin Bain (Oxford University, U.K.) for invaluable discussions and mentoring, and Prof. Gabor Somorjai (UC Berkeley, U.S.A.) for inspiration and guidance while building up our SFG facility.

References and Notes

(1) Persson, D.; Leygraf, C. *J. Electrochem. Soc.* **1995**, *142*, 1468.
(2) Fukuda, Y.; Fukushima, T.; Sulaiman, A.; Musalam, I.; Yap, L. C.; Chotimongkol, L.; Judabong, S.; Potjanart, A.; Keowkangwal, O.; Yoshihara, K.; Tosa, M. *J. Electrochem. Soc.* **1991**, *138*, 1238.
(3) Leygraf. C.; Graedel, T. *Atmospheric Corrosion*; Wiley: New York, 2000.
(4) Graedel, T. E. *J. Electrochem. Soc.* **1992**, *139*, 1963.
(5) Maréchal, Y. *J. Chem. Phys.* **1987**, *87*, 6344.
(6) Bratož, S.; Hadži, D.; Sheppard, N. *Spectrochim. Acta* **1956**, *8*, 249.
(7) Krause, P. F.; Katon, J. E.; Rogers, J. M.; Phillips, D. B. *Appl. Spectrosc.* **1977**, *31*, 110.
(8) Semmler, J.; Irish, D. E. *J. Solution Chem.* **1988**, *17*, 805.
(9) Bertie, J. E.; Michaelian, K. H. *J. Chem. Phys.* **1982**, *77*, 5267.
(10) Nakabayashi, T.; Kosugi, K.; Nishi, N. *J. Phys. Chem. A* **1999**, *103*, 8595.
(11) Nakabayashi, T.; Nishi, N. *J. Phys. Chem. A* **2002**, *106*, 3491.
(12) Kosugi, K.; Nakabayashi, T.; Nishi, N. *Chem. Phys. Lett.* **1998**, *291*, 253.
(13) MacInnes, D. A.; Shedlovsky, T. *J. Am. Chem. Soc.* **1932**, *54*, 1429.
(14) Ng, J. B.; Shurvell, H. F. *J. Phys. Chem.* **1987**, *91*, 496.
(15) Tanaka, N.; Kitano, H.; Ise, N. *J. Phys. Chem.* **1990**, *94*, 6290.
(16) Génin, F.; Quilès, F.; Burneau, A. *Phys. Chem. Chem. Phys.* **2001**, *3*, 932.
(17) Semmler, J.; Irish, D. E. *J. Mol. Liq.* **1990**, *46*, 1.
(18) Nishi, N.; Nakabayashi, T.; Kosugi, K. *J. Phys. Chem. A* **1999**, *103*, 10851.
(19) Haurie, M.; Novak, A. *J. Chim. Phys.* **1965**, *62*, 146.
(20) Haurie, M.; Novak, A. *J. Chim. Phys.* **1965**, *62*, 137.
(21) Sims, R. W.; Willcott, M. R.; Inners, R. R. *J. Chem. Phys.* **1979**, *70*, 4562.
(22) Whalrafen, E. *J. Chem. Phys.* **1967**, *47*, 114.
(23) Venyaminov, S. Y.; Prendergast, F. G. *Anal. Biochem.* **1997**, *248*, 234.
(24) D'Arrigo, G.; Maisano, G.; Mallamace, F.; Migliardo, P.; Wanderlingh, F. *J. Chem. Phys.* **1981**, *75*, 4264.
(25) Carey, D. M.; Korenowski, G. M. *J. Chem. Phys.* **1998**, *108*, 2669.
(26) Du, Q.; Superfine, R.; Freysz, E.; Shen, Y. R. *Phys. Rev. Lett.* **1993**, *70*, 2313.
(27) Richmond, G. L. *Chem. Rev.* **2002**, *102*, 2693.
(28) Hirose, C.; Akamatsu, N.; Domen, K. *Appl. Spectrosc.* **1992**, *46*, 1051.
(29) Miranda, P. B.; Shen, Y. R. *J. Phys. Chem. B* **1999**, *103*, 3292.
(30) Eisenthal, K. B. *Chem. Rev.* **1996**, *96*, 1343.
(31) Bloembergen, N.; Pershan, P. S. *Phys. Rev.* **1962**, *128*, 606.
(32) Bell, R. B.; Bain, C. D.; Ward, R. N. *J. Chem. Soc., Faraday Trans.* **1996**, *92*, 515.
(33) Superfine, R.; Guyot-Sionnest, P.; Hunt, J. H.; Kao, C. T.; Shen, Y. R. *Surf. Sci.* **1988**, *200*, L445.
(34) Butcher, P. N.; Cotter, D. *The Elements of Nonlinear Optics*, *Cambridge Studies in Modern Optics: 9*; Cambridge University Press: Cambridge, 1990.
(35) Adamson, A. W.; Gast, A. P. *Physical Chemistry of Surfaces*, 6th ed.; John Wiley and Sons: New York, 1997.
(36) Baldelli, S.; Schnitzer, C.; Campbell, D. J.; Shultz, M. J. *J. Phys. Chem. B* **1997**, *101*, 10435.
(37) Gragson, D. E.; McCarty, B. M.; Richmond, G. L. *J. Am. Chem. Soc.* **1997**, *119*, 6144.
(38) Murphy, W. F.; Bernstein, H. J. *J. Phys. Chem.* **1972**, *76*, 1147.
(39) Fischer, W. B.; Eysel, H. H.; Nielsen, O. F.; Bertie, J. E. *Appl. Spectrosc.* **1994**, *48*, 107.
(40) Miranda, P. B.; Du, Q.; Shen, Y. R. *Chem. Phys. Lett.* **1998**, *286*, 1.
(41) Burneau, A.; Génin, F.; Quilès, F. *Phys. Chem. Chem. Phys.* **2000**, *2*, 5020.
(42) Pakoulev, A.; Wang, Z.; Pang, Y.; Dlott, D. D. *Chem. Phys. Lett.* **2003**, *380*, 404.
(43) Ito, K.; Bernstein, H. J. *Can. J. Chem.* **1956**, *34*, 170.
(44) Tyrode, E.; Johnson, C. M.; Baldelli, S.; Leygraf, C.; Rutland, M. W. *J Phys Chem. B* **2005**, *109*, 329.